RESEARCH ARTICLE

PAMM
Proceedings in Applied
Mathematics and Mechanics

The impact of binding energies on the necessary conditions in aerosol deposition

Bahman Daneshian[1] | **Frank Gärtner[2]** | **Wolfgang E. Weber[1]** | **Hamid Assadi[3]** | **Thomas Klassen[2]**

[1]Chair of Structural Analysis, Helmut Schmidt University/University of the Federal Armed Forces, Hamburg, Germany

[2]Institute for Materials Science, Helmut Schmidt University/University of the Federal Armed Forces, Hamburg, Germany

[3]Brunel Centre for Advanced Solidification Technology, Brunel University London, Uxbridge, UK

Correspondence
Bahman Daneshian, Chair of Structural Analysis, Helmut Schmidt University / University of the Federal Armed Forces, Holstenhofweg 85, 22043 Hamburg, Germany.
Email: daneshba@hsu-hh.de

Abstract

Aerosol deposition (AD) enables the formation of dense ceramic coatings by high velocity impact of submicron-sized particles. However, up to now, it is still not clear how the material properties of the ceramic powder particles influence their impact behavior and possible success in layer build-up in AD. Therefore, in order to provide a broader understanding, this study utilizes molecular dynamic (MD) simulations to investigate the impacts of single-crystalline particles while manipulating binding energies, particle sizes, and impact velocities, addressing a rather wide range of different materials and process conditions. The findings reveal that increasing binding energies from 0.22 to 0.96 eV necessitates up to three times higher velocities to reach thresholds for bonding and fragmentation, which are linked to potential layer formation. For conditions above the velocity thresholds given by individual binding energies, similarities in the deformation and fragmentation patterns are derived. Consequently, rough estimations regarding the required particle impact velocities for AD of different materials can be inferred.

KEYWORDS
aerosol deposition, binding energy, impact simulation, molecular dynamics, nanoparticle

1 | INTRODUCTION

The Aerosol Deposition method (AD) is a promising technique for creating ceramic coatings on various substrate materials, covering metals, ceramics, and polymers. AD involves accelerating submicron to some micron-sized ceramic particles (ranging from 200 nm to 5 μm) in a carrier gas flow to velocities of 100–600 m/s before they impact the substrate in a vacuum chamber. This method aims to achieve ceramic coatings with properties comparable to or even better than the bulk material, to their nanocrystalline state [1]. Hence, the method allows for constructing microdevices [2] which can be used beneficially in structural health monitoring [3].

One of the key influences observed in AD concerns the tuning of impact velocities to create coatings for different ceramic powders. The needed impact velocities increase with the mechanical properties and the sintering temperature of the ceramic material. For instance, hard ceramics like alpha-alumina require 150–500 m/s velocities, while softer ceramics

like lead zirconate titanate require lower velocities of 100–300 m/s to achieve coating formation [2]. According to the literature, a threshold velocity exists for each specific material in AD, which depends on its specific properties and powder particle size, and to a certain extent also on substrate properties [2, 4]. Experimental and simulation studies have validated this threshold velocity concept. Further investigations [1] have also explored the influence of softer and harder ceramic powders on the coating microstructures: successful formation of dense, pore-free coatings is usually associated with the occurrence of refined grains in sizes of 10–30 nm.

Research on the mechanical properties of particles used in AD primarily aims at understanding and optimizing their impact velocity by considering factors such as particle size, density, shape and associated effects on kinetic energy and drag forces in the AD process [4–6]. However, several uncertainties remain regarding the influence of the mechanical properties on the impact behavior of single-crystalline particles. Molecular dynamics (MD) simulations and analytical models have revealed the formation of cone-shaped deformed regions and shear cracks at the particle-substrate interface during particle bonding [5]. The mechanical properties of the material affect the occurrence and possible sizes of these regions, as well as the density and length of cracks and even grain refinement. The density and length of meridional and shear cracks play a significant role in particle fragmentation, but their exact influence on the shape and size of the bonded region remains unclear.

To address these issues, a comprehensive investigation was conducted using MD simulations to deduce general trends for AD of ceramic materials. The different mechanical properties of various ceramic materials were introduced by modified LENNARD-JONES (M-LJ) potentials. To reduce computational time, a simplified 2-D model was established. This might restrict the extraction of exact data but should allow for deriving trends. The study is focused on analyzing individual impact behaviors while examining deformation and fracture patterns and observing temperature evolution within single-crystalline, brittle particles in AD. Parameters such as particle binding energy, impact velocity, and particle size were varied to gain insights into different aspects of the AD process and the behavior of ceramic particles with diverse characteristics.

2 | METHODS

In this study, MD simulations are used to investigate phenomena during tensile tests and particle impact using simplified two-dimensional models. To capture material brittleness, a M-LJ potential according to Equation (1) was employed [5]. Deviating from the usual LENNARD-JONES descriptions, the M-LJ potential incorporates a cutoff radius r_c to account for material brittleness [5]. Different material properties were induced by systematically altering the binding energies represented by the energy parameter ϵ. To represent YOUNG's moduli of various soft and hard engineering ceramics commonly used in AD, binding energies of 0.22, 0.45, 0.65, and 0.96 eV were applied as ϵ values. Structural lengths in the M-LJ potential were considered by $\sigma = 2.23$ Å, $r_c = 3.345$ Å $= 1.5\,\sigma$. The atomic configurations for testing were created as single crystalline close-packed (11) face-centered cubic (fcc) planes. LAMMPS software was utilized for the MD simulations [7]. The plane-strain condition was applied in all 2D MD simulations too. The equations of motions in the MD simulations were integrated by a timestep size of 5 fs.

$$M - LJ = \begin{cases} \epsilon\left[\left(\frac{\sigma}{r}\right)^{12} - \left(\frac{\sigma}{r}\right)^{6}\right] & \text{if } r/\sigma < r_c \\ 0 & \text{if } r/\sigma \geq r_c \end{cases} \tag{1}$$

Tensile testing simulations were performed to determine YOUNG's modulus of the different model materials and validate brittleness under varying binding energies. Each model has a rectangular shape with dimensions of 100 nm × 35 nm, see Figure 1. Deformation was applied on opposite sides along the X-axis at a constant velocity of 0.1 m/s. Periodic boundary conditions were employed in the X and Y axes to allow for a free movement of atoms, eliminate size effects on stress-strain curves and model the bulk behavior of each material. The models were initially equilibrated at room temperature (300 K) under the Canonical ensemble. Stress-strain curves were obtained by measuring and summing up the atomic stress tensors in the X direction over the entire tensile model.

As illustrated in Figure 2, the models for particle impact simulations consisted of single-crystalline rigid substrates and single-crystalline particles in sizes of 50 and 300 nm. These particles and substrates were cut from a large single-crystalline atomic plane. The measurement of lengths here is based on the equilibrium distance between two atoms in the M-LJ potential which is approximately 2.5 Å. For simplicity, the substrates and particles shared the same atomic
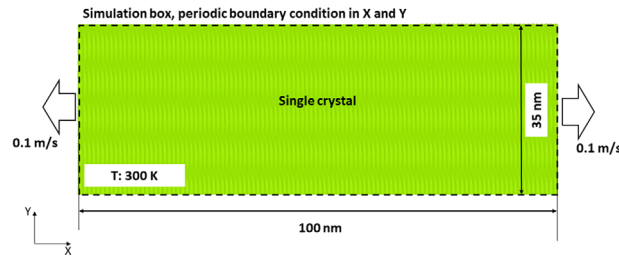
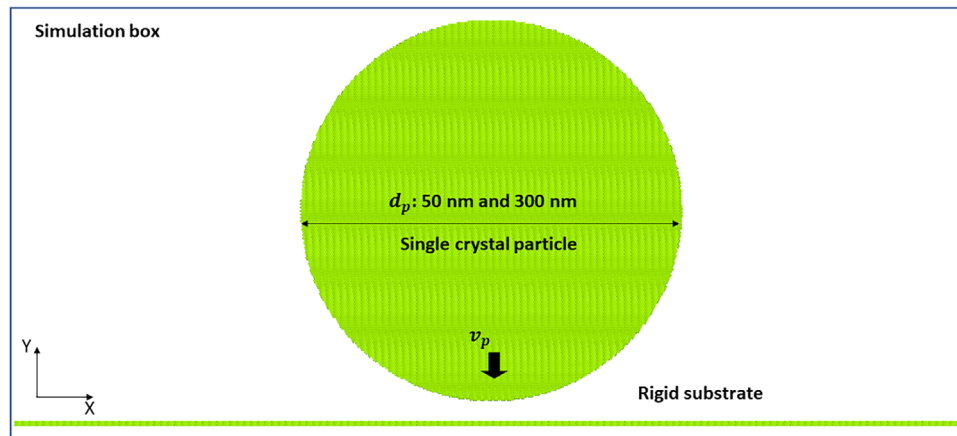**FIGURE 1** Model set-up for 2D tensile test simulations.

FIGURE 2 Model set-up for 2D impact simulations. The single crystalline particles collide with an impact velocity of vp onto a rigid substrate.

structure and orientation (epitaxy). Before impact simulations, the nanoparticles were equilibrated at room temperature for several picoseconds and then projected onto the substrates at a 90° angle with a velocity of 600 m/s. This velocity was high enough to see a wide range of impact behaviors in all selected types of particles with different binding energies. The Velocity VERLET algorithm was employed for integrating the equations of motion, and atomic shear strain analysis using OVITO software [8] was applied to study the particle impact behavior and resulting deformation patterns.

The OVITO [8] software was also utilized to employ atomic shear strain analysis, aiming to investigate the behavior of particle impact and the resulting deformation patterns. To calculate the 2D maximum atomic shear strain, three components of the atomic strain tensor were utilized according to Equation (2). In this equation, e_{ij} represents entries of the (atomic) strain tensor in the X, Y, and XY directions. The atomic strains are determined by evaluating the relative motion of neighboring atoms within a specified cut-off space.

$$\text{max. atomic shear strain} = \sqrt{\left(e_{XY}^2 + \frac{(e_X - e_Y)^2}{2}\right)} \tag{2}$$

LAMMPS [7] was also used to calculate the particles' temperature distribution fields. To accomplish this, the particle domain was divided into multiple rectangular bins throughout the simulation period, allowing for the analysis of the local temperature fields by examining the kinetic energy associated with each bin. This methodology is based on the established literature [5]. By comparing the changes in local temperature fields across various regions of the colliding particles, valuable insights can be gained regarding the highest temperature reached during the particle collision in AD.

3 | RESULTS

The influence of the binding energies on the mechanical properties of the M-LJ potential materials is investigated by their respective tensile stress-strain curves as given in Figure 3. The stress-strain curves reveal that the slopes representing
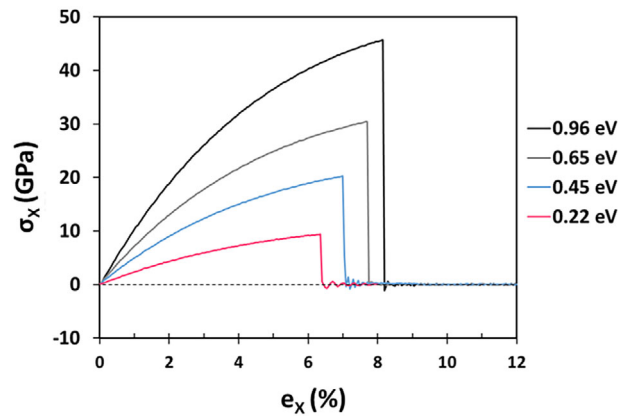
FIGURE 3 Simulated stress-strain curves of brittle materials with different binding energies. The deformation in X direction was applied by 0.1 m/s during the analyses in opposite directions.
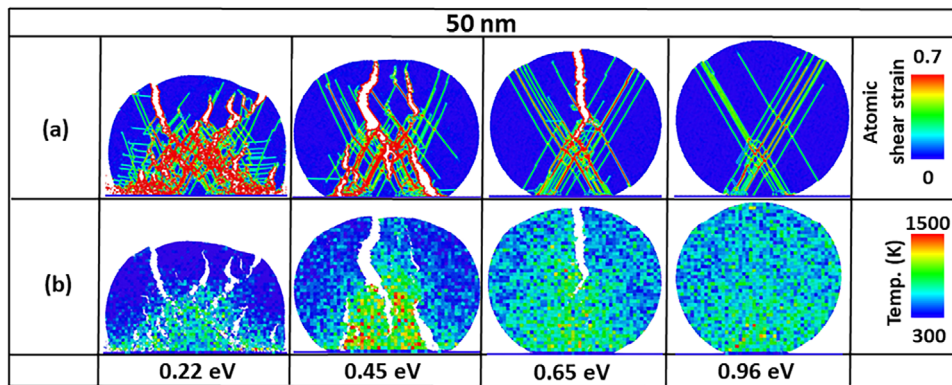

FIGURE 4 Simulated impact morphologies along with the associated shear strain fields (A) and the local temperature fields (B) of the 50 nm particles under varied binding energies (0.22, 0.45, 0.65, and 0.96 eV) 20 ps after a collision at 600 m/s.

the YOUNG's moduli and the maximum attainable stresses increase with binding energies. The observed high maximum stresses at the yield/fracture point of the M-LJ materials are attributed to their defect-free single-crystal structures, here nearly reaching the theoretical strength.

Particle impact scenarios were subsequently modeled for four binding energies, selected particle sizes, and initial velocities. The following details of impact morphologies are only given for typical examples to illustrate differences in (i) deformation behavior and (ii) temperature patterns. Here, particle sizes of 50 and 300 nm (Figure 4 and 5) were selected to distinguish the main influences of different binding energies on possible bonding or fragmentation features in different particle sizes. The selected velocity of 600 m/s corresponds to the maximum impact velocity in AD. Also, it covers possible bonding phenomena given for the different binding energies.

Figure 4A presents the simulated (i) impact morphologies with (ii) the atomic shear strain fields simultaneously to supply information on the particle's impact behaviors, deformation patterns and even reasons for possible fragmentation. Snapshots of Figure 4 were all taken after 20 ps from the impact time. According to the Figure 4A two types of impact behaviors are seen for the 50 nm particles with different binding energy values at 600 m/s: the fragmentation behavior is predominant in particles with binding energies of 0.22, 0.45, 0.65 eV, while in the particle with the highest binding energy of 0.96 eV only the bonding behavior without any fragmentation occurs. Furthermore, the lower the binding energy, the more severe fragmentation with more cracks is observed. Cracks in the lower part of the particle created by the applied shear stress during collisions of the particles, are further defined as "shear cracks". Cracks that appear in the top part of the particles in parallel with the impact directions are further defined as "meridional cracks". Snapshots of Figure 4A show that the number of meridional or shear cracks both increase with decreasing binding energy. The atomic shear strain in Figure 4A also reveals that plastic deformation within the particles is concentrated in distinct shear bands. Inside particles with higher binding energies, that is, 0.65 and 0.96 eV, shear bands mostly run through the full diameter of the particle,
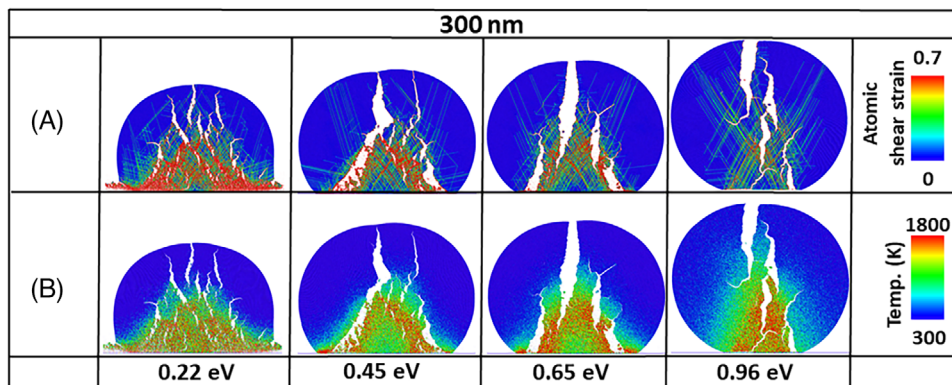
FIGURE 5 Simulated impact morphologies along with the associated shear strain fields (A) and the local temperature fields (B) of the 300 nm particles under varied binding energies (0.22, 0.45, 0.65, and 0.96 eV) 120 ps after a collision at 600 m/s. It should be noted that the temperature scale in Figure 5B is different from that in Figure 4B.

and some shear bands show higher strain, as represented by red coloring. Plastic deformation is more dominant in the lower part of the particles near the interface of the particle and substrate. Particles with lower binding energies in general show more plastic strain. Obviously, cracks are originating from these highly strained areas with the maximum shear strain values, and some then propagate all through the particle, leading to fragmentation.

Figure 4B presents the snapshots from the released local temperature fields 20 ps after the impact of the particles with different binding energies at 600 m/s. Both the shear strain fields and the local temperature fields were plotted simultaneously for a better understanding of the underlying phenomena in Figure 4A and 4B. In the particles with a binding energy of 0.22 and 0.45 eV, the local temperature increased to 900 and 1500 K, respectively, at the lower part of the particle, while almost all other areas of the particles remained at 300 K. In addition, the local temperature dissipation seemed to be restricted in the lower part of the particle by the cracks. The higher maximum temperature in the particle with the binding energy of 0.45 eV may be associated with the higher amount of total binding energy released. In the particle with the binding energy of 0.65 eV, a more uniform pattern of temperature release is seen in Figure 4B compared to particles with the binding energy of 0.22 and 0.45 eV. This uniformity is related to the lack of significant fragmentation in this particle. In the particle with the binding energy of 0.96 eV, which has no internal cracks, temperature dissipation pattern is even more uniform. The color of the temperature patterns in the particles with binding energies of 0.65 and 0.96 eV is very similar (light green color). This means that despite the amount of their binding energy, the temperature in both particles only rose to around 900 K. The previous studies revealed that the temperature released in the bonded particles depends on the impact velocity [5]. This study also revealed that the released temperature might also be independent of the particle binding energy. However, further analysis is still required to prove such a hypothesis.

Furthermore, examining the local temperature fields with the shear strain fields in the 50 nm particle in Figure 4 shows that temperatures first rise in the lower part of the particles, where maximum plastic deformation occurs. Therefore, it is justifiable to attribute the elevated local temperatures at the lower part of the particles in particles with the binding energy of 0.22 and 0.45 eV to the occurred total plastic deformation in these regions together with restricted dissipation capability due to cracking.

This result in Figure 4 motivated a detailed study of the deformation pattern and local temperature analysis in the larger particles with different binding energies at the same spraying conditions. Figure 5 shows the results of MD impact simulations for the particle size of 300 nm with atomic shear strain fields and the associated local temperature fields 120 ps after the impact. This time was sufficient to represent the particles' final shapes and accumulated deformation. For direct comparison to the results from Figure 4, the impact velocity of 600 m/s was selected in Figure 5 too.

When subjected to a velocity of 600 m/s, all 300 nm particles with binding energies ranging from 0.22 to 0.96 eV experience fragmentation behavior, although their fragmentation characteristics varied considerably. For example, the 300 nm particle with the binding energy of 0.22 is fragmented and characterized by several shear cracks at the bottom of the particle, also showing maximum flattening. In the particle with the binding energy of 0.45 eV, a lower amount of plastic deformation (the green fields) and less flattening are visible in the snapshot. Consistently, fewer cracks are also observed. This trend is basically continued by the particle with the binding energy of 0.65 eV. However, the meridional crack at the top of the particle is larger while the shear cracks at two sides of the particle are smaller. The fragmentation pattern

depends on the competition between the shear and meridional cracks created by the shear strains and X strains, respectively [5]. Consequently, in the particle with the binding energy of 0.96 eV, the meridional crack at the top of the particle becomes even larger, while the shear cracks at two sides of the particle's bottom become smaller than the particle with a lower amount of binding energies.

The shear strain pattern analysis in the 300 nm particles Figure 5A reveals that particles with lower binding energies exhibit pronounced plastic deformation at the interface between the particle and the substrate and along the shear cone towards the center. Conversely, particles with higher binding energies demonstrate less pronounced plastic deformation, primarily in areas where shear bands intersect inside the particles. Notably, the greater extent of plastic deformation observed in particles with lower binding energies leads to more cracks, limiting the propagation of cracks. Therefore, the main characteristics of particles with a size of 300 nm at 600m/s can be summarized as follows: shear strain fields and localized plasticity are more pronounced in cases of lower binding energies. Additionally, higher levels of localized shear contribute to subsequent shear fractures, competing against meridional failures. Plasticity also influences the size of deformation areas shaped like cones. When conditions are met for plastic deformation, these associated shear cones form and expand more extensively in lower binding energies. Interestingly, the material within these shear cones demonstrates less fragmentation.

Figure 5B represents the snapshots from the released local temperature fields 120 ps after the impact of the 300 nm particles with different binding energies at 600 m/s. In the 300 nm particle with the binding energy of 0.22 eV, a local temperature increase up to 1 800 K is seen in the lower part of the particle, where maximum deformation and fragmentation are seen in its shear strain field counterpart in Figure 5A, while the rest of the particle experiences only 300 K temperature. In the 300 nm particle with the binding energy of 0.45 eV, the maximum temperature of around 1 800 K is seen around the shear cracks at the bottom of the particle. This issue is associated with restricting heat dissipation to the whole parts of the particle by the shear cracks. A very similar pattern is also seen for the particle with the binding energy of 0.65 and 0.96 eV in Figure 5B. In fact, despite the amount of the binding energy, the maximum local temperature of around 1 800 K is reported for all 300 nm particles with different amount of binding energies.

4 | CONCLUSIONS

In this study, artificial brittle ceramics were created by manipulating the binding energies in the M-LJ potential. Then the impact behaviors of the created brittle materials were simulated via MD for two particle diameters of 50 and 300 nm. Comparing the impact behavior results for 50 and 300 nm particles with different binding energies revealed that 300 nm particles were all fragmented at 600 m/s, while two impact behaviors of (i) bonding and (ii) fragmentation were observed in the 50 nm particles with different binding energies. The deformation pattern in both sizes is associated with plastic deformation and shear localization at the intersection of the shear bands. Furthermore, plastic deformation mainly occurs at the lower part of the particles and the interface with the substrate in both 50 and 300 nm particles with different binding energies. The observed plastic deformation at the lower part of the particles and the interface with the substrate may be the reason for the bonding of the particles to the substrate in AD. Comparing the fragmentation patterns between the 50 and 300 nm particles with different binding energies also revealed that with increasing the diameter of the particles, fragmentation by meriodonal cracks is more dominant, which causes less amount of material remaining on the substrate. This phenomenon may justify the size limitation of the adhering particles in the AD process. However, it must always be considered that when modeling particles in 2D, they have less geometrical freedom for deformation than their 3D counterparts. This limitation leads to underestimating the deformation of the impacted particle in the direction parallel to the substrate in 2D compared to 3D. Consequently, this issue might postpone the bonding and fragmentation behaviors to a higher impact velocity regime in 2D. Thus, 2D simulations restrict the extraction of accurate data about the process. Nevertheless, they can still provide valuable information about trends and influential factors. Comparing the temperature fields between the 50 and 300 nm particles revealed that the particle's fragmentation in AD can suppress the heat generated from plastic deformation. The maximum resulting temperature in the remained material on the substrate can reach up to 1 800 K at 600 m/s in particles with different binding energies. This high temperature might also affect the bonding of successive particles and coating formation in AD via consolidation.

ORCID
Bahman Daneshian https://orcid.org/0000-0002-2139-1675

REFERENCES

1. Akedo, J. (2004). Aerosol deposition method for fabrication of nano crystal ceramic layer. *Materials Science Forum*, *449*, 43–48.
2. Akedo, J. (2008). Room temperature impact consolidation (RTIC) of fine ceramic powder by aerosol deposition method and applications to microdevices. *Journal of Thermal Spray Technology*, *17*, 181–198.
3. Rottmann, M., Roloff, T., Rauter, N., Rittmeier, L., Sinapius, M., & Weber, W. E. (2023). A numerical study on planar gradient acoustic impedance matching for guided ultrasonic wave detection. *Journal of Vibration and Control*, 1–14.
4. Hanft, D., Exner, J., Schubert, M., Stöcker, T., Fuierer, P., & Moos, R. (2015). An overview of the aerosol deposition method: process fundamentals and new trends in materials applications. *Journal of Ceramic Science and Technology*, *6*(3), 147–182.
5. Daneshian, B., Gärtner, F., Assadi, H., Vidaller, M. V., Höche, D., & Klassen, T. (2022). Features of ceramic nanoparticle deformation in aerosol deposition explored by molecular dynamics simulation. *Surface and Coatings Technology*, *429*, 127886.
6. Park, H., Kwon, H., Kim, Y., & Lee, C. (2019). Computational research on factors affecting particle velocity in a vacuum kinetic spray process. *Journal of Thermal Spray Technology*, *28*, 1945–1958.
7. Thompson, A. P., Aktulga, H. M., Berger, R., Bolintineanu, D. S., Brown, W. M., Crozier, P. S., in't Veld, P. J., Kohlmeyer, A., Moore, S. G., Nguyen, T. D., Shan, R., Stevens, M. J., Tranchida, J., Trott, C., & Plimpton, S. J. (2022). Lammps a flexible simulation tool for particle-based materials modeling at the atomic, meso, and continuum scales. *Computer Physics Communications*, *271*, 108171.
8. Stukowski, A. (2009). Visualization and analysis of atomistic simulation data with ovito – The open visualization tool. *Modelling and Simulation in Materials Science and Engineering*, *18*(1), 015012.

How to cite this article: Daneshian, B., Gärtner, F., Weber, W. E., Assadi, H., & Klassen, T. (2023). The impact of binding energies on the necessary conditions in aerosol deposition. *Proceedings in Applied Mathematics & Mechanics*, e202300275. https://doi.org/10.1002/pamm.202300275